ADVANCED MATERIALS TECHNOLOGIES
www.advmattechnol.de

Quantitatively Discriminating Alcohol Molecules by Thermally Modulating NiO-Based Sensor Arrays

Meng Li, Hongyu Liu, Junqing Chang, Tiantian Dai, Kazuki Nagashima, Zanhong Deng, Takeshi Yanagida, Xiaodong Fang, and Gang Meng**

Although temperature modulation of a single (nonselective) semiconductor gas sensor has demonstrated its great capability on discriminating gas molecules, quantitative analysis of the type and concentration of structurally similar volatile organic compounds (VOCs) molecules remains a significant challenge. In this work, as an alternative to a single oxide sensor, sensor arrays composed of four types of NiO-based sensor synchronously perform thermal modulation with a unique programmed cooling temperature profile. Apart from improved category discrimination by using entire sensor arrays, the peak temperature of the temperature profile plays an important role in distinguishing the concentration difference induced by subtle variations of the electrical responses. A high peak temperature of ≈300 °C facilitates concentration discrimination (with an accuracy ratio of 85.9%). This work highlights the importance of the peak temperature in (simultaneous) quantitative analysis of the types and concentrations of VOCs molecules with similar properties.

1. Introduction

Volatile organic compounds (VOCs) are ubiquitous in human exhalation, house decoration, industrial emissions, and transportation. Exposure to VOCs may make people dizzy or even poison them, depending on the species and concentration of VOCs. Taking alcohol groups as an example, methanol poisoning outbreaks occur frequently in developing countries because of adulterated alcohols.[1] The widely used ethanol and isopropanol (IPA) are classified as group 1 carcinogens by the International Agency for Research on Cancer of the World Health Organization.[2] The analysis of VOCs molecules using metal oxide semiconductor (MOS) gas sensors has attracted considerable interest, because of their small size, low power consumption, and easy integration.[3] Persistent efforts have been devoted to addressing the selectivity issue, a prerequisite for the real applications of MOS sensors.[4–6] Normally, it is difficult to discriminate adsorbed molecules using a single MOS sensor operated at isothermal (constant operation temperature) measurements, because of the limited extracted features (i.e., temperature-dependent sensitivity[7] and adsorption/desorption time[8]), especially for chemically and structurally similar VOCs molecules, which possess similar (reducing vapors) electrical responses.[9] Constructing electronic nose or sensor arrays with distinct surface properties by adopting new materials, extrinsic doping,[10] noble metal modification,[11] and heterogenous or composite materials[12] has been widely used to multiply the (isothermal) features, thus enriching the recognition capability of MOS sensors.[13,14] Various n-type (SnO_2,[15] ZnO,[16,17] WO_3,[18] In_2O_3[19]) based electronic noses have been reported. For example, Kang et al.[7] fabricated electronic noses with five different MOS sensors through high-resolution nanolithography and successfully distinguished seven types of hazardous vapor. Shi et al.[13] reported the precise discrimination of similar (mesitylene, *o*-xylene, and toluene) vapors using cross-reactive arrays. However, isothermal features (temperature-dependent isothermal measurements) are either insufficient or time-consuming to acquire (by minimizing the temperature interval, increasing the number of isothermal measurement cycles), which makes it difficult or insufficient to extract the subtle features of different molecules with different concentrations.

M. Li, H. Liu, J. Chang, T. Dai, Z. Deng, G. Meng
Anhui Provincial Key Laboratory of Photonic Devices and Materials
Anhui Institute of Optics and Fine Mechanics
Key Lab of Photovoltaic and Energy Conservation Materials
Hefei Institutes of Physical Science
Chinese Academy of Sciences
Hefei 230031, China
E-mail: menggang@aiofm.ac.cn

M. Li, J. Chang, T. Dai
Scinece Island Branch, Graduate School
University of Science and Technology of China
Hefei 230026, China

M. Li, Z. Deng, G. Meng
Advanced Laser Technology Laboratory of Anhui Province
Chinese Academy of Sciences
Hefei 230037, China

H. Liu, X. Fang
College of New Materials and New Energies
Shenzhen Technology University
Shenzhen 518118, China
E-mail: fangxiaodong@sztu.edu.cn

K. Nagashima, T. Yanagida
Department of Applied Chemistry
Graduate School of Engineering
The University of Tokyo
Tokyo 113-8656, Japan

The ORCID identification number(s) for the author(s) of this article can be found under https://doi.org/10.1002/admt.202100762.

DOI: 10.1002/admt.202100762

In comparison with isothermal measurements, thermal modulation varies the sensor temperature, a key parameter that affects both the adsorption and the redox kinetics of target analyte molecules and the surface reactive oxygen species (ROS) of the oxide.[20] Rich rate or kinetics-related features of adsorbed molecules can be extracted from a single MOS sensor to discriminate diverse (VOCs) molecules, even for a nonselective (commercial) n-type MOS sensor.[21] Our previous work indicated that p-type NiO outperforms commercial n-type SnO_2 sensors in terms of VOCs discrimination.[22] Lately, we have demonstrated that aliovalent Sc[23] and Sc, Li[24] (co)doping could drastically boost the electrical response of NiO sensor to ethanol and several other VOCs molecules. Apart from modified electrical properties (e.g., base resistance of sensor), the surface adsorption affinity and reactivity properties of NiO-based sensors could be tuned via aliovalent doping, which offers a route to differentiate subtle features of adsorbed VOCs species with different concentrations. Because MOS sensors are chemical sensors, and electrical responses (origin of molecular features) stem from the specific gas/MOS interfacial charge interaction. In addition, though diverse kinds of heating waveform have been reported,[25] some fundamental issues are still unclear, such as how to set the temperature range to extract the molecular features efficiently.

In this work, as an alternative to a single oxide sensor, sensor arrays composed of p-type NiO-based sensors including pure NiO, Sc-doped NiO (Sc:NiO),[23] Li-doped NiO (Li:NiO), and Sc and Li co-doped NiO (Sc-Li:NiO)[24] with modified sensing characteristics were constructed and performed thermal modulation. A programmed cooling temperature profile was synchronously applied to the sensor arrays. Probed by three kinds of alcohols (with the same functional group of –OH), methanol, ethanol, and IPA, the peak temperature of the heating waveform was systematically tuned from 50 to 300 °C to generate a series of transient electrical response signals, which were subsequently analyzed using machine learning algorithms, including principal component analysis (PCA), linear discriminate analysis (LDA), and multilayer perceptron (MLP). Present NiO-based electronic nose possesses excellent category discrimination capability and can discriminate three types of alcohol molecule with 100% confidence by MLP at all peak temperature modulations, even at a low peak temperature of 100 °C. However, concentration discrimination is sensitively dependent on peak temperature. A high peak temperature of ≈300 °C offers sufficient surface ROS to differentiate the subtle electrical response differences induced by the concentration difference and achieves a high concentration recognition accuracy ratio of 85.9%. This work demonstrates the importance of peak temperature for the simultaneous discrimination of structurally similar VOCs molecules by thermally modulating MOS sensor arrays, and it offers new avenues for exploring future advanced VOCs recognition electronics.

2. Results and Discussion

In this work, mild hydrolysis of Ni^{2+} (as well as Sc^{3+} and Li^{+}) in base solution under appropriate temperature was employed to obtain hierarchical layered structure β-$Ni(OH)_2$ microflowers.[23,24,26] Followed by a simple sintering process, a series of p-type NiO microflowers, including pure NiO, Sc:NiO, Li:NiO, and Sc-Li:NiO, could be obtained to construct sensor arrays (**Figure 1**a–d). All the NiO materials show a pure face-centered cubic NiO phase (JCPDS No. 78–0423) (Figure 1e). An enlarged scan indicates a shift of (220) peak to small diffraction angle (right of Figure 1e), suggesting an expansion of the NiO lattice due to Sc and/or Li doping, which agrees well with the fact that both Sc^{3+} (74.5 pm) and Li^{+} (76 pm) dopant have a larger ionic radius than that of Ni^{2+} (69 pm) under the same coordination number of 6.[24] In addition, there is a slight broadening of X-ray diffraction (XRD) (200) peak of Sc contained NiO materials in Figure 1e, inferring smaller average grain sizes (estimated by Scherrer formula) of Sc:NiO (15.4 nm) and Sc-Li:NiO (14.5 nm) than NiO (19.7 nm) and Li:NiO (18.9 nm). As the solubility product constant of $Sc(OH)_3$ (10^{-31}) is much smaller than that of $Ni(OH)_2$ (10^{-16}),[27] the adding of Sc^{3+} in Ni^{2+}-based precursor possibly accelerates the hydrolysis rate, and thus results in a slight size shrinking of microflowers illustrated in scanning electron microscope (SEM) images (Figure 1a–d). Additional material characterization data,

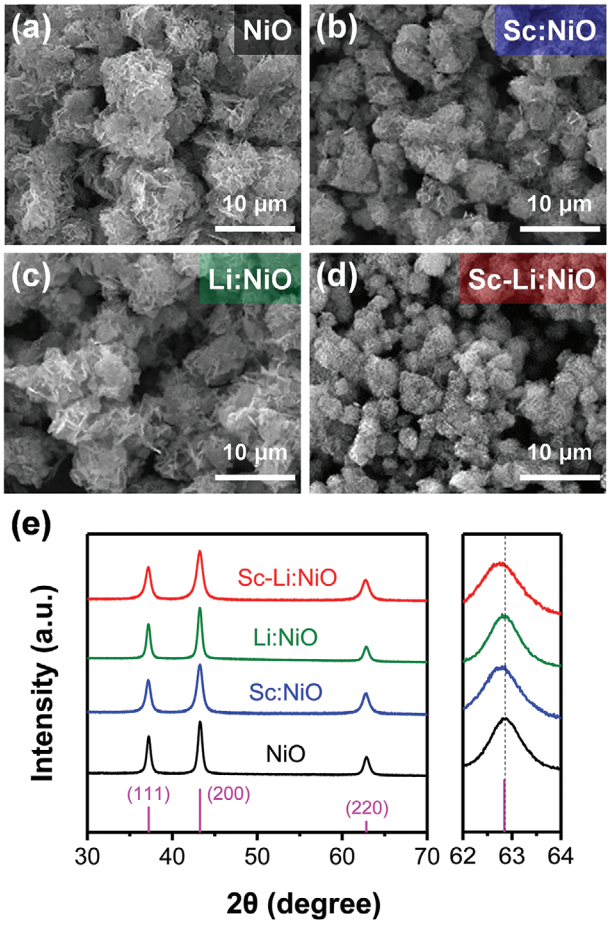

Figure 1. SEM images of a) NiO, b) Sc:NiO ($Ni_{0.98}Sc_{0.02}O$, 1.6 at% Sc), c) Li:NiO ($Ni_{0.94}Li_{0.06}O$, 5.6 at% Li), and d) Sc-Li:NiO ($Ni_{0.93}Sc_{0.02}Li_{0.05}O$, 1.8 at% Sc + 5.3 at% Li) microflowers. e) XRD patterns of the pure NiO, Sc:NiO, Li:NiO, and Sc-Li:NiO, the right shows an enlarged XRD pattern of (220) peak.

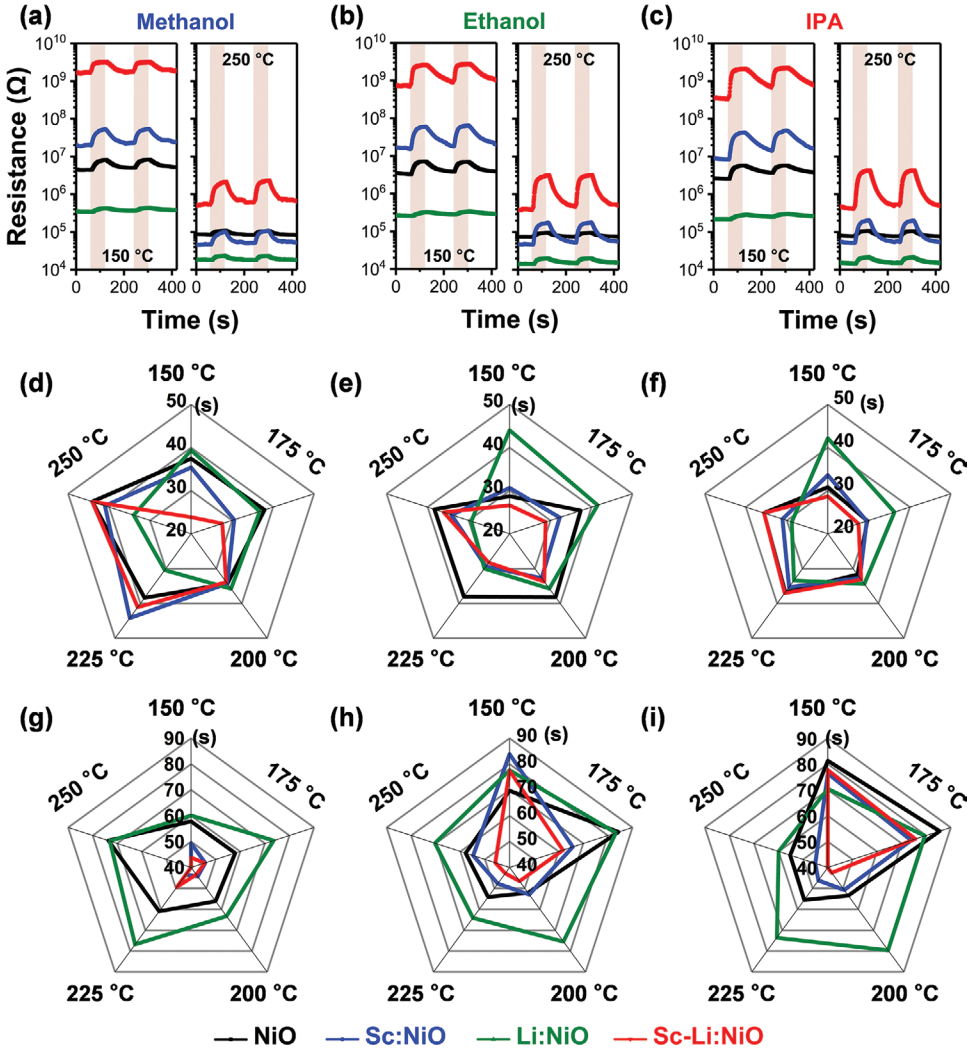

Figure 2. Variations of four series of NiO-based sensor resistances upon successive exposure to 200 ppm a) methanol, b) ethanol, c) IPA at operation temperature of 150 and 250 °C. Radar plot for the response times of four series of NiO-based sensors to 200 ppm d) methanol, e) ethanol, and f) IPA, and recovery time to 200 ppm g) methanol, h) ethanol, and i) IPA at operation temperatures ranging from 150 to 250 °C.

including transmission electron microscopy, X-ray photoelectron spectroscopy, electron paramagnetic resonance spectroscopy, and energy dispersive X-ray spectroscopy, can be found in our previous works.[23,24]

The isothermal sensing characteristics of four kinds of NiO-based sensors toward alcohol molecules have been investigated first (**Figure 2** and Figure S1, Supporting Information). Aliovalent Sc, Li, and Sc-Li doping could alter the electrical properties (base resistance, R_{air}) of the sensing channel (Figure 2a–c). As the widely used shallow acceptor for p-type NiO,[28,29] Li doping allows to increase the conductivity (reduce the base resistance) of p-type NiO. On the contrary, high valence Sc^{3+} cations may introduce additional donor states, resulting in an increase of base resistance (Figure 2a–c). In comparison with Li dopant, Sc and Sc-Li dopants are supposed to create more surface active sites (i.e., ROS) in NiO and contribute to higher electrical responses to alcohols.[23,24] The differences in the total available surface active sites are beneficial for concentration discrimination, which is discussed later. The response time (Figure 2d–f) and recovery time constants (Figure 2g–i) suggest a difference in the surface redox reaction and recovery rate of methanol, ethanol, and IPA molecules on NiO-based materials. Sc-Li:NiO sensor possesses a higher response (Figure S2, Supporting Information) and a relatively shorter response/recovery time than that of undoped NiO (Figure 2d–i) at the same operation temperature. Meanwhile, regarding the same Sc-Li:NiO sensor, the optimal operation temperature shifts from ≈225 °C (methanol) to 200 °C (IPA) and 175 °C (ethanol), implying a difference in the reducibility of alcohol groups with different numbers of carbon chains, which leads to differences in the rate of the redox reaction on the surfaces of sensitive materials.[30]

Although the isothermal measurements of the NiO sensor arrays (Figure 2a–c and Figure S2, Supporting Information) show different temperature-dependent sensing characteristics, limited features (steady response, response time, and recovery time) obtained by one measurement cycle (taking ≈200 s in Figure 2a–c), hinder the discrimination of the tested alcohol molecules. The temperature modulation of a single sensor

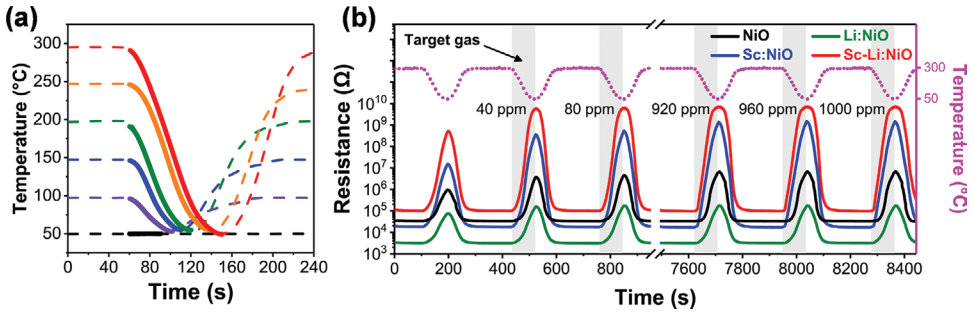

Figure 3. a) One cycle of temperature modulation profile with varied initial temperatures (50–300 °C) and a fixed ending temperature of 50 °C, the programmed cooling temperature waveforms used in this work are shown by solid lines. b) Resistance variations of NiO-based sensor arrays upon successive exposure to various IPA gases (40–1000 ppm, 40 ppm step) under the periodic programmed cooling temperature modulation profiles from 300 to 50 °C (dash magenta line). Gas response signals during cooling stage (light gray zones) were utilized for the subsequent feature extraction.

demonstrated its efficiency and capability for molecule feature extraction,[22,31] as illustrated by the recognition performance comparison between temperature modulation and isothermal testing (Figure S3, Supporting Information). Because temperature plays a crucial role in the adsorption and subsequent redox reactions of adsorbed molecules with MOS surfaces,[20] appropriately selecting the temperature range for temperature modulation is critical for fully exploring the discrimination capability of an MOS sensor. In this work, programmed cooling temperature waveforms with varied initial temperatures (50–300 °C) and a fixed ending temperature (50 °C) have been proposed (solid lines in **Figure 3**a), exhibiting an improved recognition performance (Figure S4, Supporting Information) than heating or periodic heating–cooling down waveforms widely used in previous works.[32] The peak temperature was systematically varied from 300 to 50 °C to modulate the recognition performance of the NiO sensor arrays. The transient resistances of the sensor arrays under successive programmed temperature cooling (to 50 °C) and heating (to 300 °C) cycles (dash magenta line in Figure 3b) upon exposure to 40–1000 ppm IPA vapors (light gray zones) are depicted in Figure 3b. A slight increase in the sensor resistance at 50 °C with increasing IPA concentration agrees well with the isothermal responses of p-type NiO sensors. All the sensors could be fully refreshed after the heating and high-temperature maintenance stages (dash plateau magenta line in Figure 3b), as indicated by the stable base resistance (before alcohol vapor injection). Moreover, differing from previous temperature modulation reports widely using n-type SnO_2-based sensors, present p-type NiO sensors show a large temperature coefficient of resistance/resistivity, which inevitably introduces dominant variation of sensor resistance (two to five orders), purely arising from the intrinsic electrical property of the sensing channel, irrespective of the adsorbed molecules. Using sensitivity data (R_{gas}/R_{air}) instead of resistance data has proved to be a key step in extracting the intrinsic features of adsorbed molecules from thermal modulation data.[22]

Figure 4 and Figure S5 in the Supporting Information present the normalized response of the sensor arrays toward three types of alcohol vapor with different concentrations, under various peak temperatures. At a constant low temperature of 50 °C, the responses of all sensors were rather noisy, arising from fewer thermally generated carriers (or high resistance) in NiO-based sensing channels. Tiny electrical responses at low temperature (50 °C) (see Figure S2, Supporting Information) indicate negligible VOCs/oxide interfacial redox reactions, which hinder subsequent recognition. Increasing the peak temperature facilitates the generation of surface ROS,[33] which subsequently participate in the oxidation reaction with adsorbed reducing vapors (i.e., VOCs)[20,33] and contributes to the increase in the electrical response upon exposure to alcohol vapors. Therefore, the normalized responses of the four sensors increased first (Figure 4 and Figure S5, Supporting Information), and then decreased because of less generated ROS at low temperatures. This trend can be seen clearly in Figure S6 and Table S1 in the Supporting Information. Sc-Li:NiO sensor arrives at the peak response earlier (30 s for 40 ppm methanol at a peak temperature of 200 °C) than the other three sensors because of the high and prompt response at 200 °C (Figure S6, Supporting Information) and negligible response at 50 °C (Figure S7, Supporting Information). The NiO and Li:NiO sensors possess a longer time constant (≈68 and 247 s, respectively) under the same conditions (Figure S6, Supporting Information), owing to the relatively high response at 50 °C (Figure S7, Supporting Information) and the long response, recovery times at both high temperature (Figure S6, Supporting Information) and 50 °C (Figure S7, Supporting Information). With increasing concentration of alcohol vapor, a gradual (left) shift in the normalized response curves was observed (rainbow colored curves in Figure 4 and Figure S5, Supporting Information) for all sensors, which contain the rich features related to the concentration of tested VOCs vapors. Moreover, the rainbow curves have a large span with an increase in the peak temperature (Figure 4 and Figure S5, Supporting Information), inferring improved concentration features, which are discussed later. The distinct transient response characteristics, endowed by the altered surface physical and chemical properties of NiO materials by aliovalent doping, undoubtedly multiply the features of test VOCs molecules and thus benefit molecule discrimination by machine learning algorithms.

A supervised LDA algorithm was first applied to reduce the multidimensional feature vector into a 2D visual space, as shown in **Figure 5**. Except at the constant temperature of 50 °C and high peak temperature of 300 °C, methanol (blue square), ethanol (green circle), and IPA (red triangle) species could be clearly separated from other types of gas molecule by analyzing the response signals obtained from temperature modulation. Although the performance of a single sensor at different peak

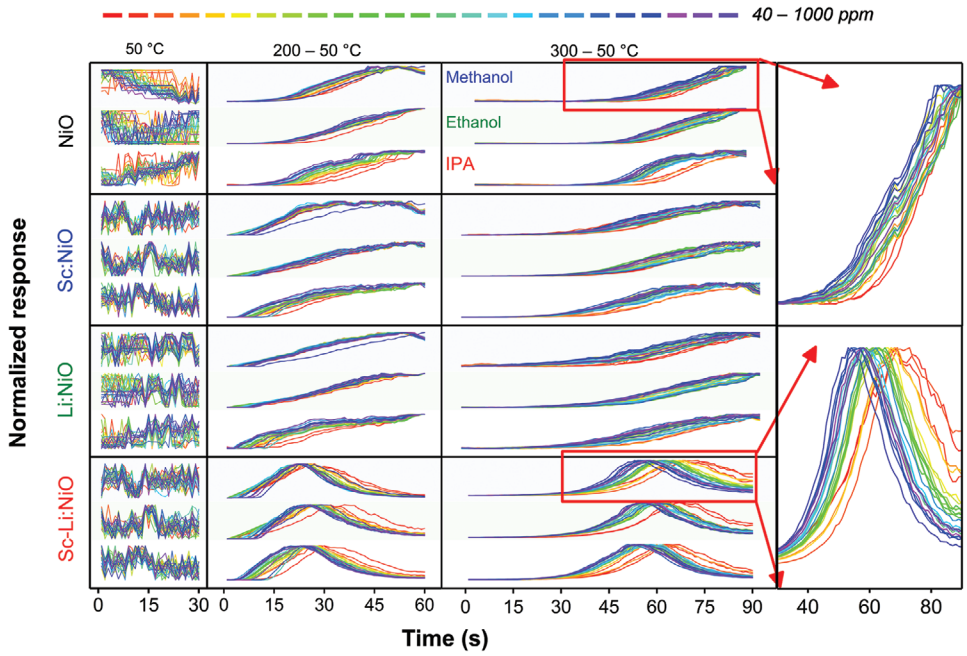

Figure 4. Normalized response curves upon exposure to 40–1000 ppm alcohol vapors during the programmed cooling stage.

temperatures varied, the recognition capability of the sensor arrays outperforms all four sensors at any peak temperature (Figure S8, Supporting Information). More interestingly, even a low peak temperature of 100 °C (≈100 °C lower than the optimal operation temperature in Figure S2, Supporting Information) is capable of classifying alcohol types. The powerful discrimination capability of low peak temperature-modulated (NiO) sensor arrays promises a future low-power-consumption electronic nose, providing new opportunities for diverse environmental and health monitoring.

Next, the alcohol concentrations were analyzed quantitatively. The input concentration (40–1000 ppm) was split into

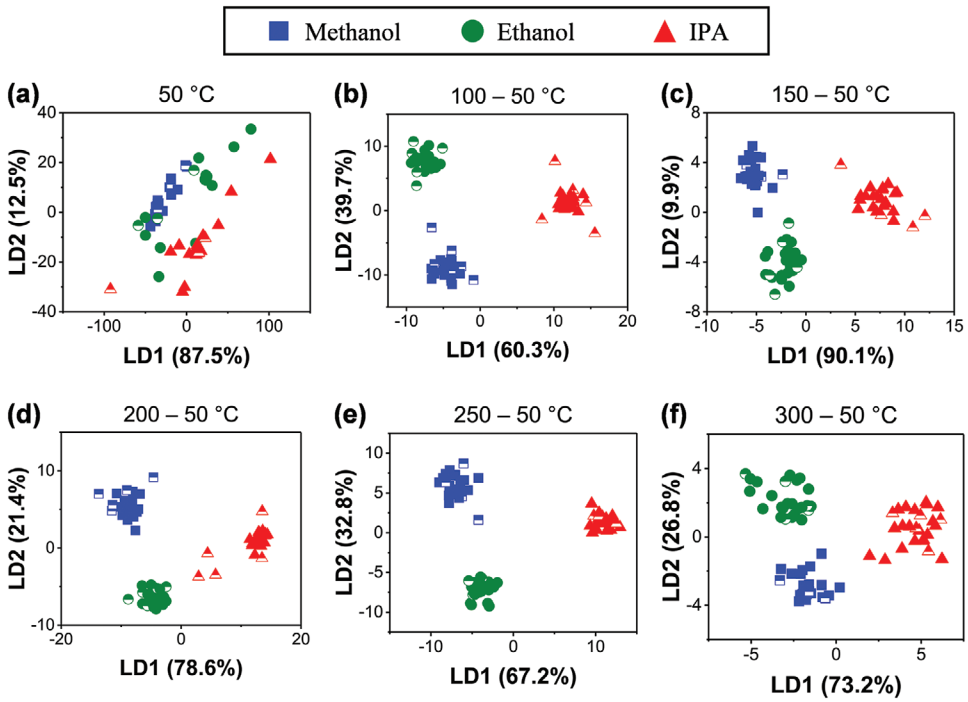

Figure 5. The 2D feature space of LDA mapping of species classification based on features extracted from entire sensor arrays at the peak temperatures of a) 50, b) 100, c) 150, d) 200, e) 250, and f) 300 °C. The half-filled markers indicate test sets carried out in independent experimental sessions. (LD1 and LD2 are the discriminant scores of the first two linear discriminant functions with the largest contribution to classification) (25 samples of each analyte).

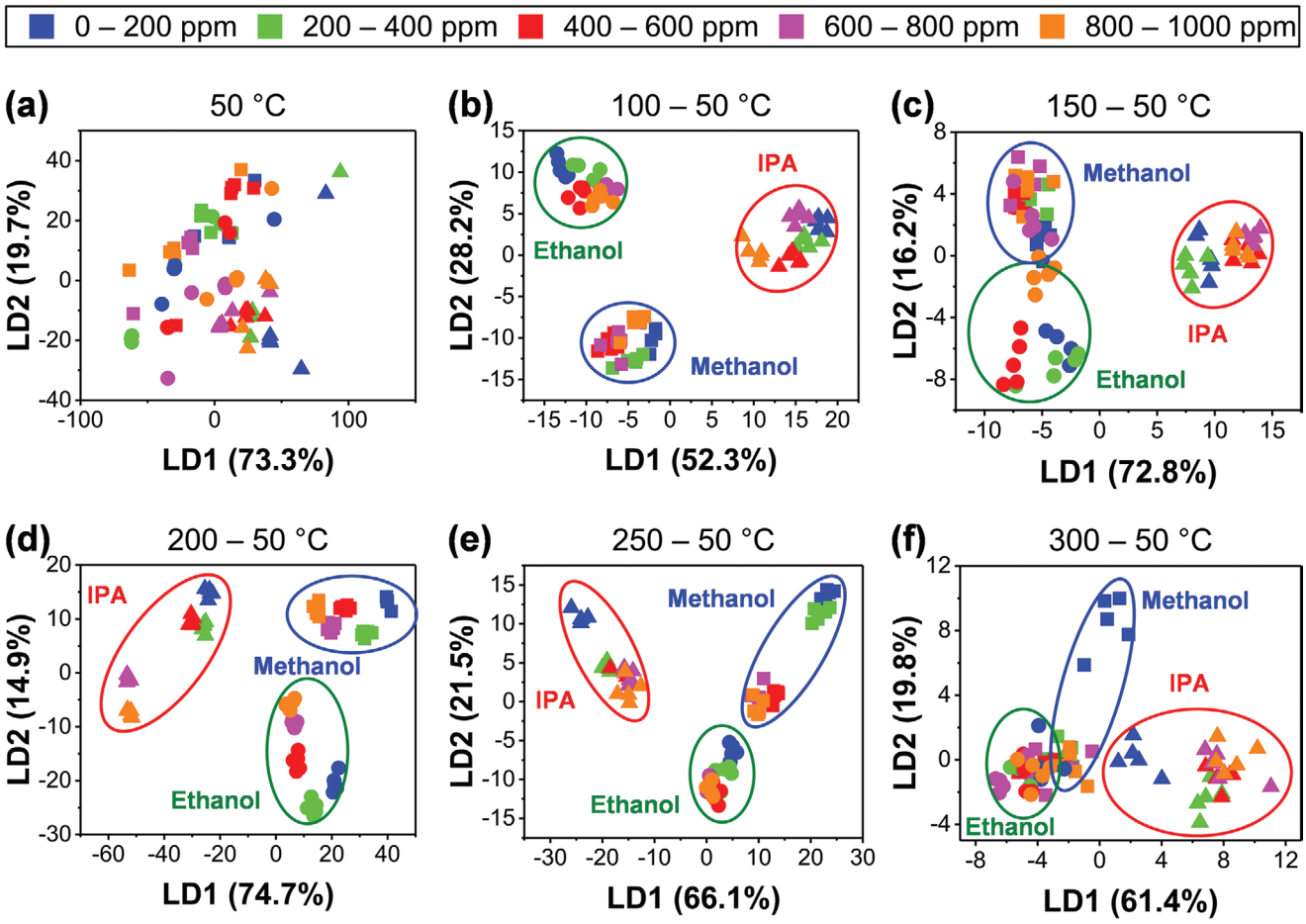

Figure 6. The 2D feature space of LDA mapping of concentration classification based on entire sensor arrays at peak temperatures of a) 50, b) 100, c) 150, d) 200, e) 250, and f) 300 °C. (LD1 and LD2 are the discriminant scores of the first two linear discriminant functions with the largest contribution to classification) (25 samples of each analyte).

five intervals, and the gas molecules in a specific concentration interval were regarded as a single category. The LDA concentration classifications under various peak temperatures are shown in **Figure 6**. The peak temperature plays an important role in species discrimination (shown as the nonoverlapping of three-shaped frames in the feature space). When the peak temperature is 200 °C, the points of different colors in each frame are separated more clearly, indicating that the species and concentration discrimination at the peak temperature is most effective. Under low peak temperature modulation, molecular features are not easily extracted owing to the low gas response.

To evaluate the effect of peak temperature on the correct recognition rate, an MLP neural network was used. Consistent with the LDA classification (Figure 5), species classification can be accomplished easily for all the peak temperatures ranging from 100 to 300 °C, and the correct ratio is higher than 75%, even when using a small number (4% of the total) of samples as the training set (the remaining 96% of the samples are used as the testing set), as shown in **Figure 7**. When the peak temperature increased, the correct recognition rate first increased and then decreased, reaching the highest value at about 200 °C. Confusion matrix analysis (Figure S9, Supporting Information) indicates that the highest mean correct recognition rate of 87.7%

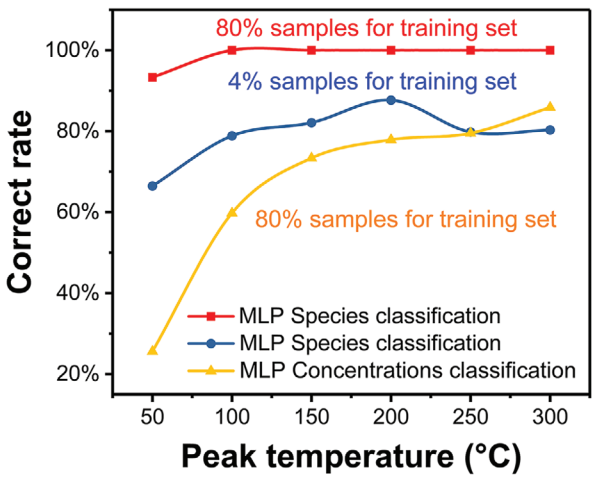

Figure 7. Correct recognition rate versus peak temperature for species classification of 80% of samples for training set (red line), species classification of 4% of samples for training set (blue line), and concentration classification of 80% of samples for training set (yellow line) (25 samples of each analyte).

occurred at the peak temperature of 200 °C, with the lowest error rates indicated by a higher transparency of the pink color, which agrees well with the PCA classification (Figure S10, Supporting Information). On the contrary, the correct ratio for concentration recognition is much smaller than that for category recognition, even when 80% of the total samples were used as the training set (Figure 7), indicating a potential overlap of concentration-related features. Moreover, the correct ratio monotonically increased with the peak temperature, and the recognition capability of the sensor arrays outperforms all four sensors at any peak temperature (Figure S11, Supporting Information).

Clarifying the variation in electrical responses during temperature modulation is essential for the rational design of high-performance electronic noses. The increased surface unsaturated oxygen vacancy defects induced by Sc^{3+} dopant were generally regarded as active sites for catalytic oxidization of adsorbed VOCs molecules, which greatly enhance the electrical response toward VOCs molecules.[23] Regarding Sc and Li co-dopant, density functional theory suggests that ethanol molecules could preferentially binding with alkali Li^{+} sites in comparison with Ni^{2+} sites,[24] results in a drastic improvement of electrical responses toward ethanol. We suppose that altering the surface reactivity of NiO-based sensors via doping, either enhancing or suppressing, results in the distinct interfacial redox kinetics, which contributes to the electrical features of tested VOCs with different concentrations. In addition to the intrinsic temperature-dependent resistance of the semiconductor, the resistance variation of the NiO-based sensor could be modulated by both ionosorption (reaction (2))[33] and surface redox reactions between ROS (O_2^-) adsorbed VOCs molecules (note that physisorption typically does not account for significant resistance variation of an MOS sensor[20]). Under an ambient air atmosphere, the ionosorption of adsorbed O_2 (greatly activated by increasing the operation temperature[33]) extracts minority electron carriers from p-type NiO and causes a decrease in resistance via the following reactions

$$O_{2\,gas} \rightarrow O_{2\,ads} \quad (1)$$

$$O_{2\,ads} + e^- \rightarrow O_2^- \quad (2)$$

Ionosorption generates surface ROS O_2^- ions, which enable to oxidize the adsorbed alcohol (such as methanol) molecules via two possible reaction pathways[34]

$$2CH_3OH_{ads} + O_2^- \rightarrow 2HCHO + 2H_2O + e^- \quad (3)$$

$$2CH_3OH_{ads} + 3O_2^- \rightarrow 2CO_2 + 4H_2O + e^- \quad (4)$$

The injection of free electrons into the NiO-based sensing layers via reactions (3) and/or (4) results in an increase in the sensor resistance. The electrical response of the sensor depends on the concentration of adsorbed alcohol molecules and ROS, both of which depend on the temperature. It is well known that raising the temperature facilitates the generation of ROS.[33] Raising the operating temperature (from room temperature) usually enhances the electrical responses, while a temperature that is too high enhances the desorption of preadsorbed analyte alcohol molecules.[35] Therefore, a volcano response versus temperature curve with an optimal operating temperature is commonly exhibited, as shown in Figure S2 in the Supporting Information. The varied response kinetics, including the isothermal temperature-dependent responses (Figure 2a–c) and response and recovery time constants (Figure 2d–i) indicate the different surface redox kinetics between the tested alcohol molecules and (doped) NiO. Such a difference is essential for contributing to the electrical response differences or intrinsic features of different VOCs molecules with varied concentrations under appropriate temperature modulations.

To gain insight into the misclassified groups, a confusion matrix analysis of concentration recognition under different peak temperatures was performed (**Figure 8** and Figure S12, Supporting Information). Under a low operation temperature (50–100 °C), most of the misclassified samples (pink) are neighboring concentration samples of the same gas. The correct recognition rate (noted by the main diagonal of the matrix) increases with elevating the modulated peak temperature (Figure 8b). At a high peak temperature, more ROS could be generated in the air atmosphere. These ROS would be gradually or rapidly consumed (via reactions (3) and (4)) during the programmed cooling stage when alcohol vapors are injected.

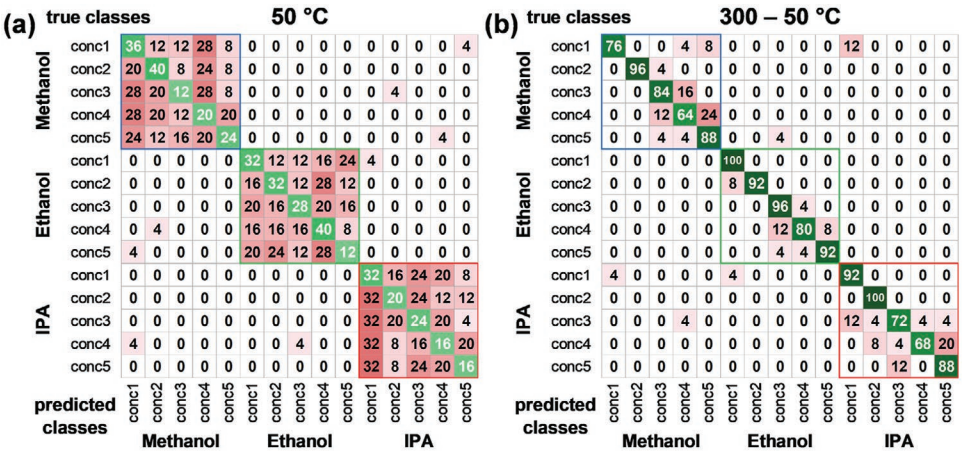

Figure 8. Confusion matrix of MLP concentrations classification based on entire sensor arrays at peak temperatures of a) 50 and b) 300 °C (25 samples of each analyte).

The onset and decay of the normalized peak response depend on the supply rate (or concentration) of alcohol vapors. Higher-concentration alcohols feed alcohol and consume ROS faster than the low-concentration alcohols, resulting in a faster increase (and decay) of the normalized response, which is the reason for forming the rainbow curves in Figure 4 and Figure S5 in the Supporting Information. At a high peak temperature, a relatively long programmed cooling time (Figure 2d) offers additional ROS and enlarges the shift of the normalized responses of different concentration analytes (rainbow colors in Figure 4 and Figure S5, Supporting Information), and the features of alcohol group gas concentrations can be effectively distinguished based on species classification. Furthermore, additional two low-concentration categories (conc1: 1–10 ppm, conc2: 10–20 ppm) were examined using sensor arrays. The MLP results (Figure S13, Supporting Information) indicate poor recognition performance in such a low-concentration range (with small electrical responses). Quantitative analysis of trace (i.e., < 10 ppm) VOCs molecules by thermally modulating the electronic nose with a higher response and/or low detection of limit will be another interesting topic beyond the scope of the present work.[36–38]

3. Conclusion

All in all, using a programmed cooling temperature waveform, the effect of peak temperature on the discrimination capability of a thermally modulated NiO-based electronic nose has been investigated, probed by three kinds of alcohol VOCs with different concentrations. It was found that category classification can be readily achieved at any peak temperature modulation (even at a low peak temperature of 100 °C). The concentration features are closely related to the peak temperature. A high peak temperature of ≈300 °C facilitated the concentration classification with an accuracy ratio of 85.9% in a large concentration range (40–1000 ppm). The possible underlying mechanism during temperature modulation was discussed to provide inspiration for the rational design of advanced VOCs molecule recognition electronics in future for diverse emerging applications.

4. Experimental Section

Synthesis and Characterization of NiO-Based Sensitive Materials: The NiO-based materials were synthesized via a wet chemical method, and detailed procedures can be found in previous works.[23,24] In short, 1.5 mL of $Ni(CH_3COO)_2{\cdot}4H_2O$ aqueous solution (1.2491 g dissolved in 10 mL deionized water), appropriate dopant (no addition for pure NiO, 11.1 mg of $Sc(NO_3)_3{\cdot}H_2O$ for Sc:NiO, 4.59 mg of $Li(CH_3COO)_2{\cdot}2H_2O$ for Li:NiO, both of the above chemicals for Sc-Li:NiO), 0.3 mL ethylenediamine, and 9 mL NaOH aqueous solution (5.6 g dissolved in 20 mL deionized water) were mixed and stirred for 10 min. The mixed precursor was heated in an oil bath at 100 °C for 30 min with strong magnetic agitation, then washed three times with deionized water and ethanol in a centrifuge, and baked in an oven at 70 °C for 24 h. Finally, the NiO-based samples were obtained by annealing in air at 500 °C for 2 h. The morphologies of the NiO-based sensors were observed using SEM (VGA3SBH). XRD measurement were conducted using a D8 ADVANCE X-ray diffractometer, operated at 40 kV, 40 mA, and an angle of 2θ ranging from 10° to 70° to collect the crystalline characteristics of the samples.

Device Fabrication and Sensing Test: First, four kinds of NiO-based powder were dispersed in an appropriate amount of ethanol and continuously stirred for more than 1 h. The paste that formed was then coated onto the sensing ceramic substrates (with heater and test electrodes) as the sensing layer. All sensors were aged in air at ≈220 °C for 1 week before testing. Three types of alcohol group gas of methanol, ethanol, and IPA (with quite similar properties, see Table S2, Supporting Information) were selected as the target analytes. Different concentrations of alcohol group gases were obtained by mixing standard gas and dry air in any ratio, controlled by mass flow controllers (CS-200, Sevenstar Electronics Co. Ltd.). The total gas flow rate was set at 500 sccm. The gas sensing tests were carried out in a four-channel gas-sensitive measurement system (SD101, Huachuang Ruike Technology Wuhan Co. Ltd.), which allowed to measure the resistance ranging from 100 Ω to 1 GΩ with a verified accuracy of ±5.0% and an accuracy of ±18.3% for 10 GΩ, as seen in Figure S14 in the Supporting Information. The temperature of the sensor was modulated from the peak temperature (50, 100, 150, 200, 250, or 300 °C) to a fixed low temperature of 50 °C by tuning the heating voltage. The alcohol group vapors were injected into the test chamber in the temperature drop range. After the temperature modulation, raising the heater temperature and maintaining a constant peak temperature (≈120 s) facilitated the desorption of the tested analytes and recovery of the sensor baseline resistances. Before the sensors resistance under the target alcohol group gases (R_{gas}) was measured, the air resistance (R_{air}) was measured in the first temperature modulation cycle. The response of the alcohol group gases was defined as R_{gas}/R_{air}. Methanol, ethanol, and IPA, each at 25 different concentration levels (40–1000 ppm, 40 ppm ascending step), 75 analytes in total, were tested once in sequence from the second temperature modulation cycle.

Statistical Analysis: The features used to distinguish alcohol group gases were extracted through preprocessing steps. For each temperature modulation test, the cycle duration time was fixed, and the response value was obtained from R_{gas} divided by R_{air}, both with cycle time dimension

$$S(t) = R_{gas}(t) / R_{air}(t) \tag{5}$$

Next, the gas responses of different concentrations obtained by each temperature modulation were normalized

$$S_{nor}(t) = \left(S(t) - S_{min}\right) / \left(S_{max} - S_{min}\right) \tag{6}$$

where S_{max} and S_{min} are the maximum and minimum values of the response in the cooling range, respectively, $S_{nor}(t)$ represents the normalized response, and t is the time. Data processing was completed in Python 3.6. The features of the cycle time dimension were reduced to a 2D visual space using PCA. In addition, LDA classified the samples based on the input features. LDA used leave-one-out cross-validation, and each example was classified by functions derived from all examples except that example. A multilayer perceptron was a type of feedforward neural network proposed to solve nonlinear problems that could not be solved by a single-layer perceptron. MLP was a simple neural network, which allowed to quantitatively evaluate the features of electrical responses obtained under different peak temperatures. The features of the four sensors were input to the MLP with a hidden layer, and the number of units in the output layer was 3 or 15 according to species or concentration classification. Softmax and tanh were used as the activation functions of the output and hidden layers, respectively. The cross-entropy with faster convergence was selected as the cost function to evaluate the neural network model by minimizing the cost function. There were three training modes of the MLP, two of which were species classification, while one was concentration classification. For the first mode, 80% of the samples (75 samples in total) were used as the training set, and the rest were used as the test set. A fivefold cross-validation could make full use of the sample data. For the second mode, 4% of the samples were used as the training set, and

the rest were used as the test set. In other words, only one sample of each species (25 samples in total) was used as the training set, and samples of the same concentration of the three alcohol group gases were selected. Then, a 25-fold cross-validation was performed to avoid accidental errors. For the third mode, gas samples of 0–1000 ppm were divided into five concentration ranges according to a segment of 200 ppm. 80% of the samples (four samples) of a concentration range were used as the training set, and the rest were used as the test set. Fivefold cross-validation was used. The algorithms (PCA, LDA, and MLP) were implemented using IBM SPSS Statistics 26.

Supporting Information

Supporting Information is available from the Wiley Online Library or from the author.

Acknowledgements

This work was financially supported by the CAS Pioneer Hundred Talents Program of Chinese Academy of Sciences, Natural Science Foundation of Top Talent of SZTU (2020101), CAS-NSTDA Joint Research Projects (GJHZ202101), CAS-JSPS Joint Research Projects (GJHZ1891), Shenzhen Science and Technology Program (KQTD20170331115422184), and the Key Lab of Photovoltaic and Energy Conservation Materials (PECL2018QN001 and PECL2019QN005).

Conflict of Interest

The authors declare no conflict of interest.

Data Availability Statement

The data that support the findings of this study are available from the corresponding author upon reasonable request.

Keywords

NiO-based sensor arrays, quantitative discrimination, simultaneous classification of type and concentration, temperature modulation

Received: June 23, 2021
Revised: September 9, 2021
Published online:

[1] J. van den Broek, S. Abegg, S. E. Pratsinis, A. T. Guntner, *Nat. Commun.* **2019**, *10*, 4220.
[2] H. Xu, J. Xu, J. Wei, Y. Zhang, *Materials* **2020**, *13*, 3829.
[3] G. Meng, F. Zhuge, K. Nagashima, A. Nakao, M. Kanai, Y. He, M. Boudot, T. Takahashi, K. Uchida, T. Yanagida, *ACS Sens.* **2016**, *1*, 997.
[4] S. Y. Jeong, J. S. Kim, J. H. Lee, *Adv. Mater.* **2020**, *32*, 2002075.
[5] J. Rebholz, K. Grossmann, D. Pham, S. Pokhrel, L. Madler, U. Weimar, N. Barsan, *Sensors* **2016**, *16*, 1437.
[6] W. Hu, L. Wan, Y. Jian, C. Ren, K. Jin, X. Su, X. Bai, H. Haick, M. Yao, W. Wu, *Adv. Mater. Technol.* **2018**, *4*, 1800488.
[7] H. Kang, S. Y. Cho, J. Ryu, J. Choi, H. Ahn, H. Joo, H. T. Jung, *Adv. Funct. Mater.* **2020**, *30*, 2002486.
[8] K. Shiba, R. Tamura, G. Imamura, G. Yoshikawa, *Sci. Rep.* **2017**, *7*, 3661.
[9] T. Han, J. Yang, R. Miao, K. Liu, J. Li, D. Wang, T. Liu, Y. Fang, *Adv. Mater. Technol.* **2021**, *6*, 2000933.
[10] H. J. Kim, J. W. Yoon, K. I. Choi, H. W. Jang, A. Umar, J. H. Lee, *Nanoscale* **2013**, *5*, 7066.
[11] R. Bhardwaj, V. Selamneni, U. N. Thakur, P. Sahatiya, A. Hazra, *New J. Chem.* **2020**, *44*, 16613.
[12] Q. Zhang, C. Xie, S. Zhang, A. Wang, B. Zhu, L. Wang, Z. Yang, *Sens. Actuators, B* **2005**, *110*, 370.
[13] C. Shi, H. Ye, H. Wang, D. E. Ioannou, Q. Li, *Appl. Phys. Lett.* **2018**, *113*, 222102.
[14] Y. Gui, C. Xie, J. Xu, G. Wang, *J. Hazard. Mater.* **2009**, *164*, 1030.
[15] Y. Xu, L. Zheng, C. Yang, W. Zheng, X. Liu, J. Zhang, *ACS Appl. Mater. Interfaces* **2020**, *12*, 20704.
[16] J. Qu, Y. Ge, B. Zu, Y. Li, X. Dou, *Small* **2016**, *12*, 1369.
[17] L. Guo, Z. Yang, X. Dou, *Adv. Mater.* **2017**, *29*, 1604528.
[18] T. Lei, Q. Deng, S. Zhang, S. Cai, C. Xie, *Sens. Actuators, B* **2016**, *232*, 506.
[19] W. J. Peveler, R. Binions, S. M. V. Hailes, I. P. Parkin, *J. Mater. Chem. A* **2013**, *1*, 2613.
[20] T. Dai, G. Meng, Z. Deng, Y. Chen, H. Liu, L. Li, S. Wang, J. Chang, P. Xu, X. Li, X. Fang, *ACS Appl. Mater. Interfaces* **2020**, *12*, 37295.
[21] Q. Deng, S. Gao, T. Lei, Y. Ling, S. Zhang, C. Xie, *Sens. Actuators, B* **2017**, *247*, 903.
[22] H. Liu, Y. He, K. Nagashima, G. Meng, T. Dai, B. Tong, Z. Deng, S. Wang, N. Zhu, T. Yanagida, X. Fang, *Sens. Actuators, B* **2019**, *293*, 342.
[23] B. Tong, G. Meng, Z. Deng, J. Gao, H. Liu, T. Dai, S. Wang, J. Shao, R. Tao, F. Kong, W. Tong, X. Luo, X. Fang, *J. Alloys Compd.* **2021**, *851*, 155760.
[24] J. Chang, M. Horprathum, D. Wang, G. Meng, Z. Deng, B. Tong, P. Kidkhunthod, T. Dai, M. Li, H. Liu, W. Tong, S. Wang, X. Fang, *Sens. Actuators, B* **2021**, *326*, 128834.
[25] W. Maziarz, T. Pisarkiewicz, *Meas. Sci. Technol.* **2008**, *19*, 055205.
[26] S. Sarkar, M. Pradhan, A. K. Sinha, M. Basu, Y. Negishi, T. Pal, *Inorg. Chem.* **2010**, *49*, 8813.
[27] D. R. Lide, *CRC Handbook of Chemistry and Physics*, 87th ed., CRC Press, Boca Raton, FL **2006**.
[28] G. Fu, X. Wen, S. Xi, Z. Chen, W. Li, J.-Y. Zhang, A. Tadich, R. Wu, D.-C. Qi, Y. Du, J. Cheng, K. H. L. Zhang, K. Suganuma, *Chem. Mater.* **2018**, *31*, 419.
[29] Y.-H. Choi, D.-H. Kim, S.-H. Hong, *Sens. Actuators, B* **2017**, *243*, 262.
[30] S. Cong, T. Sugahara, T. Wei, J. Jiu, Y. Hirose, S. Nagao, K. Suganuma, *Adv. Mater. Interfaces* **2016**, *3*, 1600252.
[31] J. R. Huang, G. Y. Li, Z. Y. Huang, X. J. Huang, J. H. Liu, *Sens. Actuators, B* **2006**, *114*, 1059.
[32] Z. Mao, T. Lei, Y. He, Z. Cai, Y. Xiong, S. Zhang, *IEEE Sens. J.* **2017**, *17*, 2784.
[33] A. Gurlo, *ChemPhysChem* **2006**, *7*, 2041.
[34] K. Li, Y. Wu, M. Chen, Q. Rong, Z. Zhu, Q. Liu, J. Zhang, *Nanoscale Res. Lett.* **2019**, *14*, 57.
[35] A. Shaposhnik, P. Moskalev, E. Sizask, S. Ryabtsev, A. Vasiliev, *Sensors* **2019**, *19*, 1135.
[36] G. Peng, U. Tisch, O. Adams, M. Hakim, N. Shehada, Y. Y. Broza, S. Billan, R. Abdah-Bortnyak, A. Kuten, H. Haick, *Nat. Nanotechnol.* **2009**, *4*, 669.
[37] H. G. Moon, Y. Jung, S. D. Han, Y. S. Shim, B. Shin, T. Lee, J. S. Kim, S. Lee, S. C. Jun, H. H. Park, C. Kim, C. Y. Kang, *ACS Appl. Mater. Interfaces* **2016**, *8*, 20969.
[38] A. Bag, N. E. Lee, *Adv. Mater. Technol.* **2021**, *6*, 2000883.